Published in final edited form as:
Invest Ophthalmol Vis Sci. 2007 August ; 48(8): 3594–3601. doi:10.1167/iovs.06-1239.

Myofiber Length and Three-Dimensional Localization of NMJs in Normal and Botulinum Toxin–Treated Adult Extraocular Muscles

Andrew R. Harrison[1], **Brian C. Anderson**[1], **LaDora V. Thompson**[2], and **Linda K. McLoon**[1,3]

[1]Department of Ophthalmology, University of Minnesota, Minneapolis, Minnesota

[2]Department of Physical Medicine and Rehabilitation, University of Minnesota, Minneapolis, Minnesota

[3]Department of Neuroscience, University of Minnesota, Minneapolis, Minnesota

Abstract

Purpose—The density and three-dimensional localization of neuromuscular junctions (NMJs) of normal and botulinum toxin–treated normal adult rabbit and monkey extraocular muscles (EOMs) were analyzed. To demonstrate average myofiber length, randomly selected individual myofibers were reconstructed and compared with total muscle length.

Methods—Normal adult rabbit and monkey EOM and normal adult rabbit tibialis anterior were dissected in their entirety, frozen, sectioned longitudinally, and immunostained for NMJ localization. In addition, adult rabbit EOMs were injected with 5 U botulinum toxin, and NMJ density was determined after 2 weeks. NMJ locations for the three groups of EOM were reconstructed, and density of NMJ was determined. Individual myofibers were reconstructed from the orbital and global layers to determine mean fiber length.

Results—NMJs were dispersed throughout the entire length of all EOMs examined from adult rabbits and monkeys and were visualized by alpha-bungarotoxin staining and three-dimensional reconstruction of serial sections. In leg muscle, two relatively tight bands of NMJs were seen. Botulinum toxin significantly increased total NMJ density. Mean fiber lengths were 1.9 and 4.83 mm in the orbital and global layers, respectively, approximately 10% and 24% of the total origin-to-insertion muscle lengths. In addition, individual myofibers continuously changed their intrafascicular relationships over their lengths.

Conclusions—The density and distribution of NMJs in normal EOMs are more extensive than previously described. Individual myofibers are significantly shorter than the tendon-to-tendon muscle length in both muscle layers. Botulinum toxin results in a doubling of NMJ density. NMJ localization in normal EOMs has ramifications for understanding eye movement control, but it is also important when surgical or pharmacologic intervention is used for the treatment of strabismus, nystagmus, or other eye muscle disorders

The distribution of neuromuscular junctions (NMJs) in limb skeletal muscles of vertebrates has been described for many muscles. In general, most limb skeletal muscles have discrete, narrow motor endplate zones. Most NMJs in adult skeletal muscles are generally found in the approximate middle third of the tendon-to-tendon length of the muscle. Most craniofacial muscles diverge from this generalized plan of single motor endplate zones. In a study of 10 facial muscles, three major patterns of motor endplate zone localization were

Corresponding author: Linda McLoon, University of Minnesota, Department of Ophthalmology, Lions Research Building, Room 374, 2001 6th Street SE, Minneapolis, MN 55455; mcloo001@umn.edu.

Disclosure: **A.R. Harrison**, None; **B.C. Anderson**, None; **L.V. Thompson**, Allergan (F); **L.K. McLoon**, Allergan (F)

described[1]: one predominant motor endplate zone with two or three small zones evenly spread across the muscle, as in the zygomaticus major; two to four motor endplate zones located in eccentric positions, as in the levator labii superioris; multiple clusters of motor endplates distributed across the entire muscle, as in the orbicularis oculi.[1,2] This last pattern has also been described in laryngeal muscles.[3] Thus, motor endplate distribution is distinctly different between craniofacial muscles and limb skeletal muscles.

In general, studies of NMJ distribution in extraocular muscles (EOMs) have focused on visualizing and quantifying the en plaque and en grappe endings through the use of cholinesterase histochemistry[4,5] or autoradiography,[6] with a focus on the pattern of innervation on single myofibers. The distribution of NMJs is complicated by the presence of multiple innervated fibers in the orbital and global layers of adult EOM. However, it should be emphasized that multiple innervated fibers are in fact a minority, constituting only 7% to 20% of the myofibers in the orbital layer and 10% to 20% of the myofibers in the global layer.[7–9] Whole muscle analyses of NMJ distribution within EOM used cholinesterase histochemical procedures to visualize the junctions but did not examine complete three-dimensional reconstructions.[10,11] In the present analysis, the three-dimensional locations of all α-bungarotoxin–positive NMJs were mapped along the complete origin-to-insertional length of superior rectus muscles from normal adult rabbits and monkeys in every 10th section through the entire muscle. The extensive characterization in the present study is critical because the location of NMJs within normal EOM is important for understanding motor control of eye movements and for understanding when surgical or pharmacologic intervention is required for the treatment of strabismus, nystagmus, or other eye muscle disorders.

Botulinum toxin paralyzes NMJs and is routinely used as a treatment for strabismus and other muscle contractile disorders.[12] Studies have shown that muscle activity returns in part because of terminal nerve sprouting in the paralyzed muscle.[13] The extent of this change in terms of NMJ density within botulinum toxin–treated EOM is unknown. Thus, we examined alterations in the normal three-dimensional patterning of NMJs 2 weeks after a single injection of botulinum toxin in adult rabbit EOM.

Analyses of the length of individual myofibers relative to the whole muscle tendon-to-tendon length have described the orbital layer as containing fibers that run the entire length of the muscle and global fibers as being shorter than full muscle length.[10] However, individual myofibers have not been specifically examined and reconstructed. With the use of serially sectioned cross-sections, individual myofibers can be observed and reconstructed unequivocally. We reconstructed a number of randomly selected myofibers in normal adult rabbit EOM to determine their lengths proportionate to total muscle length.

Materials and Methods

Adult New Zealand white rabbits were obtained from Bakkom Rabbitry and housed in Association for Assessment of Laboratory Animal Care–approved animal facilities at the University of Minnesota. Monkey EOMs were obtained as waste tissue from macaque monkeys with Institutional Animal Care and Use Committee approval. All eye muscles came from normal monkeys used as controls. All procedures adhered to the ARVO Statement for the Use of Animals in Ophthalmic and Vision Research and the guidelines of the National Institutes of Health on the use of animals in research and were approved by the Institutional Animal Care and Use Committee at the University of Minnesota.

Normal adult rabbits were anesthetized with ketamine and xylazine (10 mg/kg, 2 mg/kg), and proparacaine drops were placed in the conjunctival cul-de-sac. One randomly selected

superior rectus muscle received an injection of 5 U botulinum toxin in 100 μL sterile isotonic saline. After 2 weeks, all animals were anesthetized deeply with ketamine and xylazine, followed by barbiturate anesthesia overdose or thoracotomy and exsanguination. The orbit was opened superiorly, and the superior rectus muscles were removed completely from their scleral insertion to their origin in the orbital apex. Additionally, the tibialis anterior muscles were removed from four normal adult rabbits from origin to insertion. The muscles were pinned to their in situ length in embedding molds and were surrounded by tragacanth gum, frozen in methylbutane, chilled to a slurry on liquid nitrogen, and stored at −80°C until sectioned and processed. Muscles were sectioned completely in the longitudinal plane at 12 μm, and sections were mounted on gelatin-subbed microslides. Every 10th section for the EOM and every 20th section for the tibialis anterior were immunostained for the presence of NMJs using α-bungarotoxin conjugated to Alexa Fluor 488 (Molecular Probes, Eugene, OR) at a concentration of 1:100. Slides were coverslipped with mounting medium (Vectashield; Vector Laboratories., Burlingame, CA) and were analyzed the same day they were immunostained. Monkey muscles were obtained after the monkeys were humanely killed by our collaborators. Monkey muscles were treated exactly as were rabbit muscles. Four muscles were analyzed for each species and for each experimental time point: four rabbit control extraocular muscles, four rabbit control tibialis anterior muscles, four monkey control extraocular muscles, and four rabbit muscles injected with botulinum toxin 2 weeks before examination.

NMJs in the muscle sections were visualized under a microscope (DMR; Leica Microsystems, Wetzlar, Germany). With the use of image analysis software (Topographer program, NovaPrime; Bioquant, Nashville, TN), the area of the entire muscle in longitudinal section was measured at 1.5×. Every NMJ was located at 20× and marked with X and Y coordinates recorded in the software program. This analysis was repeated for every 10th section through the entire superior rectus. The program (Topographer program, NovaPrime; Bioquant) was used to reconstruct the entire muscle, including the area outlines and locations of each NMJ. This allows for a three-dimensional reconstruction of all the NMJs in their actual X, Y, and Z locations within the entire muscle. Four normal rabbits, four normal monkeys, and four botulinum toxin–treated superior rectus muscles were reconstructed.

Density of the NMJs was calculated by determining the number of NMJs per cubic millimeter. Statistical significance between the density of NMJs in the normal and botulinum–toxin treated muscles was calculated using an unpaired *t*-test aided by statistical software (Prism and StatMate; GraphPad, San Diego, CA). An F test was used to verify that the variances were not significantly different. Data were considered significantly different if $P \leq 0.05$.

Individual myofibers from the control superior rectus muscles were reconstructed using the image analysis software (Topographer program, NovaPrime; Bioquant). Individual myofibers were chosen randomly from one of three positions within the muscle cross-section: the orbital layer, the boundary of the orbital and global layers, and the global layer. In general, they were selected from the middle one third of the width of the muscle cross-section rather than the lateral edges. If the myofiber chosen could not be traced definitively throughout its length because of section folding or tearing or other histologic artifact, another fiber was chosen. Fiber areas were manually traced, and serially sectioned muscles were used to follow the myofibers proximally and distally to their terminations. At least 10 myofibers were reconstructed from each layer, allowing for three-dimensional reconstruction of single myofibers and determination of their total length by multiplying the number of sections that contained the myofiber by the thickness of the cryostat sections. Mean fiber length was determined, and statistical significance was determined using an unpaired *t*-test as described.

Results

In all normal superior rectus muscles examined from rabbit and monkey, NMJs were found along the entire length of each muscle, from the scleral insertion to the muscle origin in the apex (Figs. 1A, 2, 3). There was no obvious endplate zone in any of the reconstructed muscles. No obvious pattern of NMJ distribution could be discerned, in contrast to tibialis anterior muscles (Fig. 4). In normal adult tibialis anterior muscles, two narrow endplate zones were clearly apparent in these whole-muscle reconstructions (Fig. 4).

After botulinum toxin injections in the rabbit superior rectus muscles, the density of the NMJ increased (Figs. 1B, 5). In addition, the individual NMJs appeared smaller than the uninjected control muscles, but individual NMJ lengths and areas were not determined (Fig. 5).

The density of NMJs was calculated based on numbers of NMJs counted and section thickness for the superior rectus muscles from the normal rabbits and monkeys and from the botulinum toxin–treated muscles from rabbits. Average density of the NMJs in rabbit superior rectus was 2777 ± 179 /mm^3, which was similar to that seen in monkey superior rectus muscles (2593 ± 106 /mm^3). In distinct contrast to the extraocular muscles, the average density of NMJs in adult rabbit tibialis anterior was 18.9 ± 0.54/mm^3 (Fig. 6), a 100-fold difference from the densities seen in normal extraocular muscle. Botulinum toxin treatment caused a significant change in NMJ density. Two weeks after injection of 5 U botulinum toxin in the rabbit superior rectus, the density of NMJs doubled to 6557 ± 700/mm^3 (Fig. 6).

Individual myofibers were reconstructed from the orbital layer, from fibers at the border of the orbital and global layers, and from the global layer (Fig. 7). All reconstructed fibers were significantly shorter than the complete tendon-to-tendon muscle length (Fig. 8). In addition, individual myofibers did not stay in the same fascicle from beginning to end (Fig. 9). When fibers were observed serially, it was clear that nearest neighbors continually changed. It was also clear that individual myofibers began (e.g., fibers 9 and 10, indicated by the horizontal arrows) and ended (e.g., fiber 9, indicated by the vertical arrow) continuously (Fig. 9). Thus, for individual myofibers, fascicular organization and neighboring myofibers changed throughout their course within the muscle.

Discussion

In contrast to most adult limb skeletal muscles, NMJs in the EOMs of adult rabbits and monkeys are extensively dispersed along the entire length of the muscles, from origin to insertion. No obvious pattern of NMJ localization could be discerned in these three-dimensional reconstructions, in direct contrast to the reconstructions of the tibialis anterior muscles, where two narrow endplate zones were clearly evident. This difference is further supported by NMJ density calculations because the density of NMJs, calculated as NMJ/mm^3 in the EOM, is 100-fold higher than in the tibialis anterior muscle. A single injection of botulinum toxin results in a significant increase in the overall density of the NMJs compared with normal adult EOM, indicating that a large amount of nerve sprouting occurs within the first few weeks after botulinum toxin injection.

Most adult limb skeletal muscles, which are derived from somites in development, develop single motor endplate zones. Muscles that are bipennate, such as the gastrocnemius, can develop two or three motor endplate zones, but they are consistently located within a single motor endplate zone for each division of the muscle.[14] Very long muscles, such as sternocleidomastoid, develop an “in-series” structure with multiple endplate zones, but again these bands are tightly localized within the segmental subdivisions within these muscles.

[15,16] Interestingly, a number of parallel-fibered muscles develop more complex patterns related to short, interdigitated fibers that taper to an end within the muscle mass.[17,18] However, these muscles still develop clearly observable banding patterns of NMJs. Many of the craniofacial muscles have a more complex pattern of NMJ distribution. These patterns vary even within a similar group of muscles, such as the facial musculature,[1] where muscles innervated by the same motor nerve develop distinct patterns of NMJ localization. Some of the facial muscles have one main endplate zone, such as the zygomaticus major, whereas others have more dispersed patterns of NMJs, such as the orbicularis oculi.[1,2] These patterns vary between humans and other vertebrates for the cricoarytenoid and thyroarytenoid muscles of the larynx, which have focal bands in rabbits and rats and dispersed distribution within these muscles in humans.[19] EOMs appear to be at the far end of this continuum relative to NMJ localization.

Several reports in the literature have investigated patterns of NMJ localization in the EOM of various species. With the use of cholinesterase histochemistry in mouse EOM, a central zone of NMJs of the en plaque type and a more widespread distribution of en grappe endings were observed throughout the muscle.[11] Other studies in rat and mouse demonstrate similar localization, suggesting species differences between these small rodents and larger mammals; however, three-dimensional reconstructions were not performed.[20–22] In human EOM, more complex patterns of innervation of individual myofibers were described; 34% of the fibers had multiple endplates on individual fibers, 29% of which were not en grappe–type endings.[6] Although earlier studies of EOM using cholinesterase incubation methods described a concentration of motor endplates in the middle third of the orbital layer and five to six zones in the global layer of cat EOM, three-dimensional reconstruction of all the NMJs was not performed.[10] However, a scattered distribution of endplates was described, particularly in the global layer. In other muscles NMJ disbursement is thought to be caused by the presence of many short myofibers and the localization of NMJs in eccentric positions along the length of single myofibers.[2,6] The dispersed nature of NMJ localization is not just a function of short individual myofibers that do not run the full tendon-to-tendon length of the muscle. Sartorius, tenuissimus, and semitendinosus muscles, which all contain short fibers, still develop discrete motor endplate zones spaced at fairly regular intervals from origin to insertion.[17]

The dispersed nature of the NMJs and their density in the adult rabbit and monkey EOM provide a good visual demonstration of how short the average myofibers are within the adult EOM. This is true in orbital and global layers of the rabbit and monkey. One report indicates that orbital layers span the full tendon-to-tendon length in cats[10]; however, this was based not on fiber reconstructions but on whole muscle acetylcholinesterase staining. The presence of short, overlapping myofibers in the EOM has been described.[10,23,24] In addition, the fact that individual myofibers in the EOM are generally shorter than the full muscle length is supported by significant differences in the patterns of myosin heavy chain isoform expression along the length of individual EOMs,[25] the reconstruction of individual myofibers in this and other studies,[26,27] and the demonstration that myomyous junctions, representing overlapping non-spanning myofibers that terminate intrafascicularly, exist within the EOM.[10] It is particularly interesting that during development, production of secondary myotubes is linked to sites of innervation of the primary myotubes.[28,29] Widespread innervation may result in the formation of small myofibers dispersed based on this pattern of innervation. In addition, the EOM retains a population of activated satellite cells that fuse into existing myofibers in apparently random locations along the muscle length.[26,27] The localization of sites for this process may be related to this dispersed nature of the sites of innervation in adult EOM, either by direct induction of myoblast fusion or by providing an environment that secondarily results in fusion of these activated satellite cells into mature myofibers.

This architectural arrangement has important implications for an understanding of length-tension relationships, shortening velocities, and the development of force within the EOM. In studies of ocular convergence, muscle force was found to be paradoxically less than would be predicted based on firing rates.[30] In another series of experiments examining extraocular motor units and whole muscle contractile properties in cats and monkeys, individual motor units lost an average of 45% to 50% of their force output when they fired in concert with additional motor units.[31–33] The presence of many short fibers also may explain why force is relatively normal in the EOM after injury.[32] In addition, it suggests that motor units may be bigger than would be predicted by counting muscle fibers in a given muscle cross-section because this would be an underrepresentation of the total number of muscle fibers in each EOM.

Botulinum toxin is commonly used in strabismus to weaken the EOM,[12] and the nature of its effect on the three-dimensional localization of NMJs has not been examined. The method of action of botulinum toxin is to cleave SNAP25, which prevents the docking of synaptic vesicles containing acetylcholine, effectively paralyzing the NMJs.[34] After injection, force gradually decreases over an 18-hour period.[35] Nerve sprouting is seen as early as 2 days after botulinum toxin treatment and slowly increases over time.[36,37] This results in a supersensitivity of the muscle in the regenerative phase[38] and correlates well with our observation that a significant increase occurs in NMJ density and that the sprouted nerves appear to maintain NMJs smaller than normal. Functional return of muscle force is related to the return of original nerves to their NMJs, though in human patients who have received multiple injections of botulinum toxin, these sprouts can persist long after functional recovery has occurred.[39] These observations suggest that it may be possible to prolong the effectiveness of a single botulinum toxin injection if nerve sprouting or NMJ assembly is inhibited or delayed, which would improve the treatment of patients with focal dystonias and related motor disorders.

It is unclear what controls EOM tone and how strabismus surgery alters muscle structure and function.[40] Understanding the normal density and localization patterns of NMJs and understanding the variation in individual myofiber lengths will facilitate future studies examining whether and how these characteristics are altered in the muscles of patients with strabismus, nystagmus, and other eye muscle motor disorders.

Acknowledgments

Supported by National Eye Institute Grants EY13979 and EY11375, Allergan, Neuro-ophthalmology Research Fund, Minnesota Medical Foundation (LKM), Minnesota Lions and Lionesses, and an unrestricted grant from Research to Prevent Blindness, Inc. (Department of Ophthalmology).

References

1. Happak W, Liu J, Burggasser G, Flowers A, Gruber H, Freilinger G. Human facial muscles: dimensions, motor endplate distribution and presence of muscle fibers with multiple motor endplates. Anat Rec 1997;249:276–284. [PubMed: 9335474]
2. Lander T, Wirtschafter JD, McLoon LK. Orbicularis oculi muscle fibers are relatively short and heterogeneous in length. Invest Ophthalmol Vis Sci 1996;37:1732–1739. [PubMed: 8759340]
3. Rossi G, Cortesina G. Morphological study of the laryngeal muscles in man. Acta Otolaryngol 1965;59:575–592. [PubMed: 14343097]
4. Kupfer C. Motor innervation of extraocular muscle. J Physiol 1960;153:522–526. [PubMed: 13831112]
5. Namba T, Nakamura T, Grob D. Motor nerve endings in human extraocular muscle. Neurology 1968;18:403–407. [PubMed: 4173449]

6. Oda K. Motor innervation and acetylcholine receptor distribution of human extraocular muscle fibres. J Neurol Sci 1986;74:125–133. [PubMed: 3734834]
7. Mayr R. Structure and distribution of fibre types in the external eye muscles of the rat. Tissue Cell 1971;3:433–462. [PubMed: 18631565]
8. Salpeter MM, McHenry FA, Feng HH. Myoneural junctions in the extraocular muscles of the mouse. Anat Rec 1974;179:201–224. [PubMed: 4133495]
9. Wasicky R, Ziya-Ghazvini F, Blumer R, Lukas JR, Mayr R. Muscle fiber types of human extraocular muscles: a histochemical and immunohistochemical study. Invest Ophthalmol Vis Sci 2000;41:980–990. [PubMed: 10752931]
10. Mayr R, Gottschall J, Gruber H, Neuhuber W. Internal structure of cat extraocular muscle. Anat Embryol 1975;148:25–34. [PubMed: 1202990]
11. Carry MR, O'Keefe K, Ringel SP. Histochemistry of mouse extraocular muscle. Anat Embryol 1982;164:403–412. [PubMed: 7137587]
12. Scott AB. Botulinum toxin injection into extraocular muscles as an alternative to strabismus surgery. Ophthalmology 1980;87:1044–1049. [PubMed: 7243198]
13. Hopkins WG, Brown MC. The distribution of nodal sprouts in a paralyzed or partly denervated mouse muscle. Neuroscience 1982;7:37–44. [PubMed: 7078728]
14. Prodanov D, Thil MA, Marani E, Delbeke J, Holsheimer J. Three-dimensional topography of the motor endplates of the rat gastrocnemius muscle. Muscle Nerve 2005;32:292–302. [PubMed: 15948200]
15. Hijikata T, Ishikawa H. Functional morphology of serially linked skeletal muscle fibers. Acta Anat 1997;159:99–107. [PubMed: 9575360]
16. McLoon LK. Muscle fiber type compartmentalization and expression of an immature myosin isoform in the sternocleidomastoid muscle of rabbits and primates. J Neurol Sci 1998;156:3–11. [PubMed: 9559980]
17. Loeb GE, Pratt CA, Chanaud CM, Richmond RJ. Distribution and innervation of short, interdigitated muscle fibers in parallel-fibered muscles of the cat hindlimb. J Morphol 1987;191:1–15. [PubMed: 3820310]
18. Gaunt AS, Gans C. Serially arranged myofibers: an unappreciated variant in muscle architecture. Experientia 1992;48:864–868.
19. Lima-Rodrigues M, Valle-Fernandes A, Nunes R, Almeida A. Distribution of NMJs in laryngeal and syringeal muscles in vertebrates. Anat Rec 2006;288A:543–551.
20. Missias AC, Chu GC, Klocke BJ, Sanes JR, Merlie JP. Maturation of the acetylcholine receptor in skeletal muscle: regulation of the AChR γ-to-ε switch. Dev Biol 1996;179:223–238. [PubMed: 8873766]
21. Kaminski HJ, Kusner LL, Block CH. Expression of acetylcholine receptor isoforms at extraocular muscle endplates. Invest Ophthalmol Vis Sci 1996;37:345–351. [PubMed: 8603839]
22. Davidowitz J, Philips G, Breinin GM. Organization of the orbital surface layer in rabbit superior rectus. Invest Ophthalmol Vis Sci 1977;16:711–729. [PubMed: 885681]
23. Rubinstein NA, Porter JD, Hoh JFY. The development of longitudinal variation of myosin isoforms in the orbital fibers of extraocular muscles of rats. Invest Ophthalmol Vis Sci 2004;45:3067–3072. [PubMed: 15326122]
24. Davidowitz J, Robinson K, Jacoby J, Philips G. Myofibril size variation along the length of extraocular muscle in rabbit and rat 1: orbital layer. Tissue Cell 1996;28:63–76. [PubMed: 8907727]
25. McLoon LK, Rios L, Wirtschafter JD. Complex three-dimensional patterns of myosin isoform expression: differences between and within specific extraocular muscles. J Muscle Res Cell Motil 1999;20:771–783. [PubMed: 10730580]
26. McLoon LK, Wirtschafter JD. Continuous myonuclear addition to single extraocular myofibers in uninjured adult rabbits. Muscle Nerve 2002;25:348–358. [PubMed: 11870711]
27. McLoon LK, Rowe J, Wirtschafter JD, McCormick KM. Continuous myofiber remodeling in uninjured extraocular myofibers: myonuclear turnover and evidence for apoptosis. Muscle Nerve 2004;29:707–715. [PubMed: 15116375]

28. Duxson MJ, Usson Y, Harris AJ. The origin of secondary myotubes in mammalian skeletal muscles: ultrastructural studies. Development 1989:743–750. [PubMed: 2483685]
29. Duxson MJ, Sheard PW. Formation of new myotubes occurs exclusively at the multiple innervation zones of an embryonic large muscle. Dev Dyn 1995;204:391–405. [PubMed: 8601033]
30. Miller JM, Bockisch CJ, Pavlovski DS. Missing lateral rectus force and absence of medial rectus co-contraction in ocular convergence. J Neurophysiol 2001;87:2421–2433. [PubMed: 11976379]
31. Goldberg SJ, Shall MS. Lateral rectus whole muscle and motor units contractile measures with the extraocular muscles intact. J Neurosci Meth 1997;78:47–50.
32. Goldberg SJ, Wilson KE, Shall MS. Summation of extraocular motor unit tensions in the lateral rectus muscle of the cat. Muscle Nerve 1997;20:1229–1235. [PubMed: 9324078]
33. Shall MS, Dimitrova DM, Goldberg SJ. Extraocular motor unit and whole-muscle contractile properties in the squirrel monkey: summation of forces and fiber morphology. Exp Brain Res 2003;151:338–345. [PubMed: 12819843]
34. Blasi J, Chapman ER, Link E, et al. Botulinum neurotoxin A selectively cleaves the synaptic protein SNAP-25. Nature 1993;365:160–163. [PubMed: 8103915]
35. Dimitrova DM, Shall MS, Goldberg SJ. Short-term effects of botulinum toxin on the lateral rectus muscle of the cat. Exp Brain Res 2002;147:449–455. [PubMed: 12444476]
36. Phamphlett R. Early terminal and nodal sprouting of motor axons after botulinum toxin. J Neurol Sci 1989;92:181–192. [PubMed: 2809617]
37. Angaut-Petit D, Molgo J, Comella JX, Faille L, Tabti N. Terminal sprouting in mouse NMJs poisoned with botulinum toxin A toxin: morphological and electrophysiological features. Neuroscience 1990;37:799–808. [PubMed: 1701041]
38. Thesleff S. Supersensitivity of skeletal muscle produced by botulinum toxin. J Physiol 1960;151:598–607. [PubMed: 13837723]
39. Holds JB, Alderson K, Fogg SG, Anderson RL. Motor nerve sprouting in human orbicularis oculi muscle after botulinum A injection. Invest Ophthalmol Vis Sci 1990;31:964–967. [PubMed: 2335457]
40. Kushner BJ. Perspective on strabismus, 2006. Arch Ophthalmol 2006;124:1321–1326. [PubMed: 16966628]

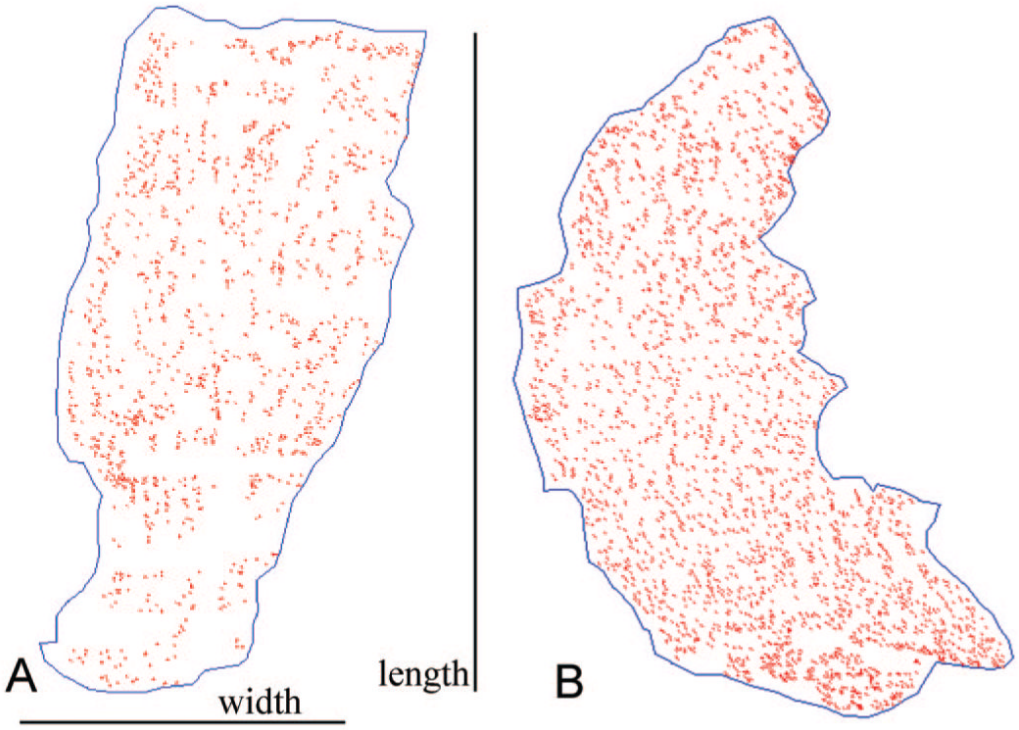

Figure 1.

(**A**) Single longitudinal section taken from the middle of the muscle thickness, and thus the global layer, of a control superior rectus muscle from a normal adult rabbit. All the NMJs marked in *red* are oriented with the origin and insertion at the *top* and *bottom* of the reconstruction. (**B**) Single longitudinal section taken from the middle of the thickness, and thus the global layer, of a superior rectus muscle from an adult rabbit 2 weeks after a single injection of 5 U botulinum toxin. All the NMJs marked in *red* are oriented with the origin and insertion at the *top* and *bottom* of the reconstruction.

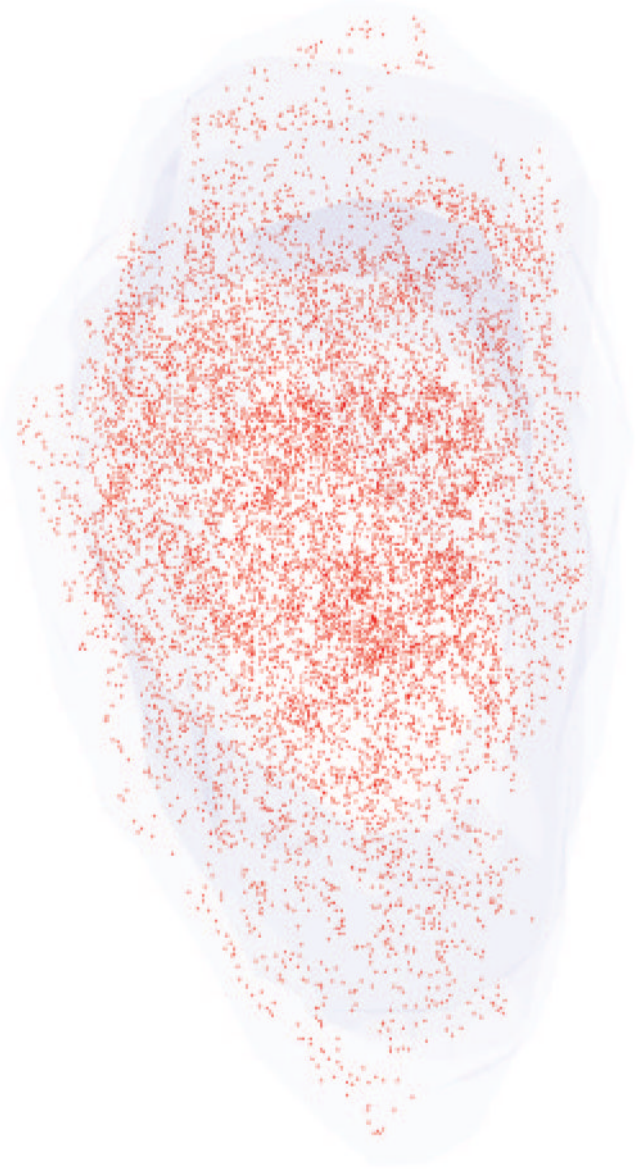

Figure 2.
Three-dimensional reconstruction of all the α-bungarotoxin–positive NMJs in every 10th section through the entire thickness of a single control superior rectus muscle from an adult rabbit. All NMJs are indicated in *red*, and the specimen is oriented with the origin and insertion at the *top* and *bottom* of the reconstruction.

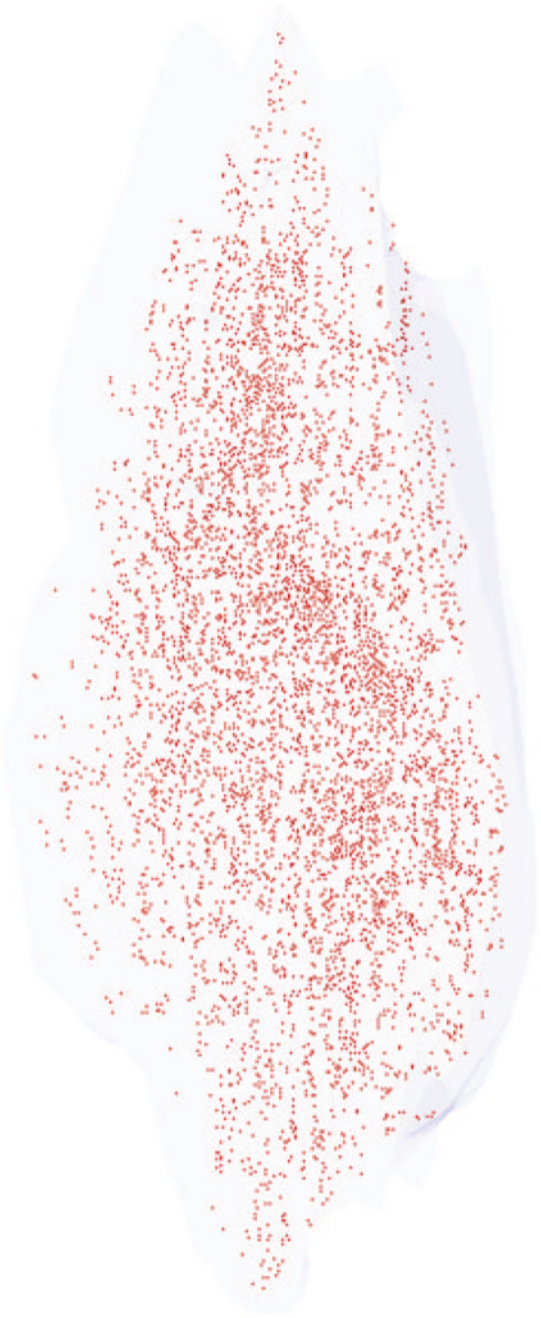

Figure 3.
Three-dimensional reconstruction of all the α-bungarotoxin–positive NMJs in every 10th section through the entire thickness of a single control superior rectus muscle from an adult monkey. All the NMJs are indicated in *red*, and the specimen is oriented with the origin and insertion at the *top* and *bottom* of the reconstruction.

Figure 4.
Three-dimensional reconstruction of all the α-bungarotoxin–positive NMJs in every 20th section through the entire thickness of a single control tibialis anterior muscle from an adult rabbit. All the NMJs are indicated in *red*, and the specimen is oriented with the origin and insertion at the *top* and *bottom* of the reconstruction. *Inset* is an example of an α-bungarotoxin–labeled NMJ. Total length of rabbit tibialis muscle is approximately 5.5 cm.

Figure 5.
Three-dimensional reconstruction of all the α-bungarotoxin–positive NMJs in every 10th section through the entire thickness of a single superior rectus muscle from a rabbit 2 weeks after a single injection of 5 U botulinum toxin. All the NMJs are indicated in *red*, and the specimen is oriented with the origin and insertion at the *top* and *bottom* of the reconstruction.

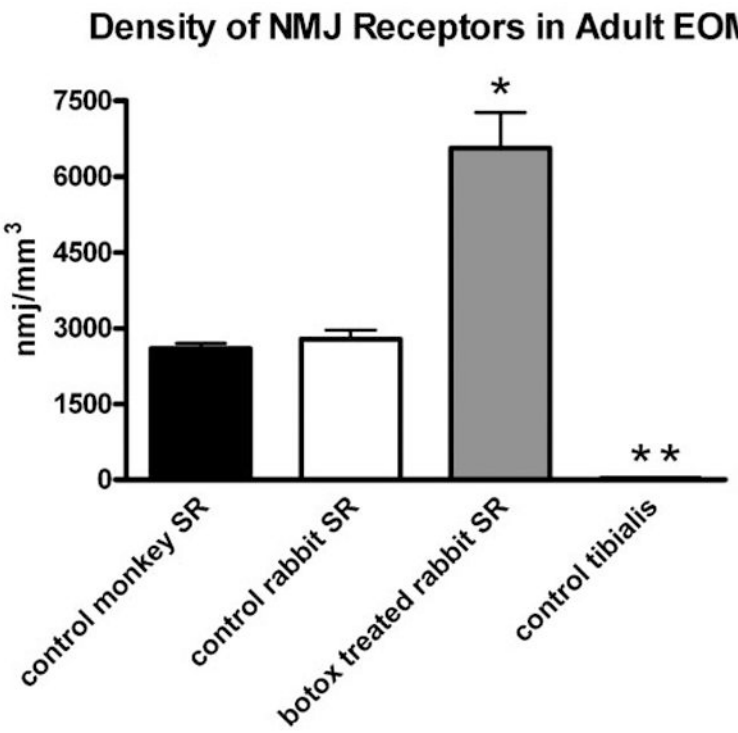

Figure 6.
Graph of the mean NMJ density in cubic millimeters in control monkey (*black*), control rabbit (*white*), and botulinum toxin–treated (*gray*) superior rectus (SR) muscles. *Significant difference from control at $P < 0.005$. **Density is low ($18.9 \pm 0.54/mm^3$) and thus is not clearly visible when graphed compared with NMJ density within the normal EOM of rabbit and monkey.

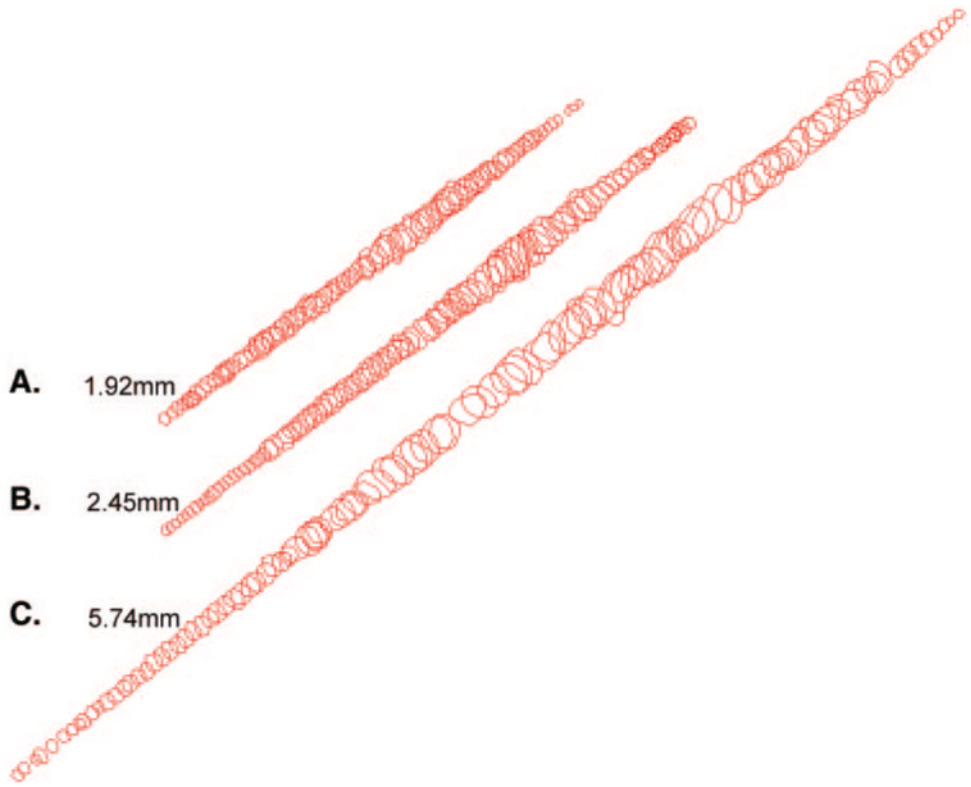

Figure 7.
Representative examples of individual myofibers reconstructed from the (**A**) orbital layer, (**B**) global layer directly contiguous with the orbital layer, and (**C**) middle of the global layer. These represent the complete lengths of these three fibers followed in serial sections.

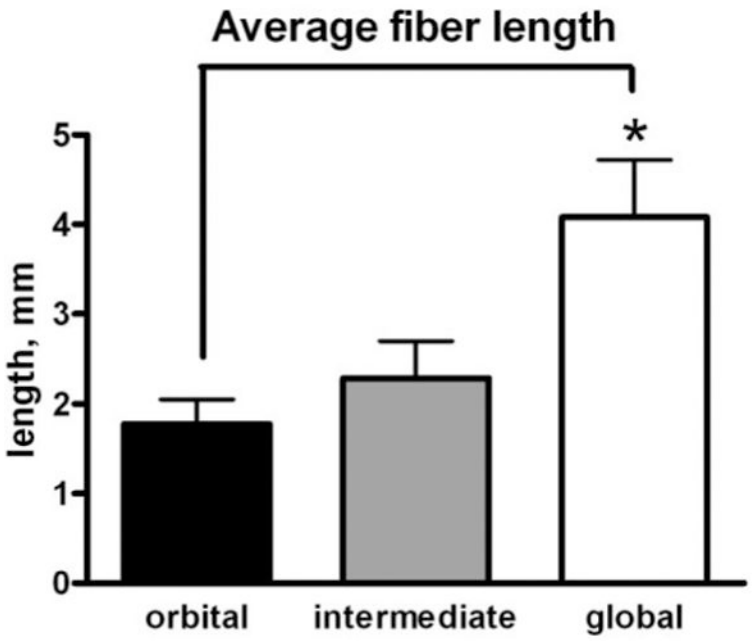

Figure 8.
Mean myofiber length, in millimeters, of individual myofibers reconstructed from the orbital layer (*black*), global layer directly contiguous with the orbital layer (*gray*), and middle of the global layer (*white*). *Significant difference from orbital and intermediate layer fibers compared with fibers from the middle of the global layer ($P < 0.005$).

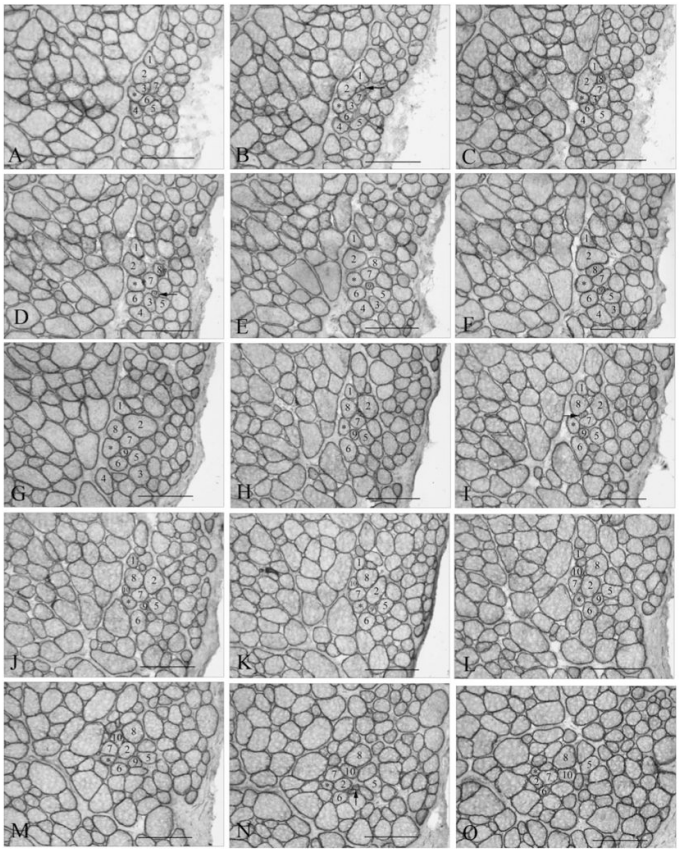

Figure 9.

(**A–O**) Representative photomicrographs of a single fiber from an adult normal superior rectus muscle (4.622 mm long) from rabbit, demonstrating changes in its fascicular relationship with its neighboring fibers relatively often in the course of its fiber length. *Individual myofiber that was reconstructed. Numbered fibers allow observation of the changes in the neighboring muscle fibers over the course of 2.9 mm represented by these selected sections. *Horizontal arrows* indicate fibers that newly appear in the cross-sections within 2.9 mm of the reconstruction (numbers 9 and 10). *Vertical arrow* indicates a fiber that ends within 2.9 mm.